Effect of Resistive Wall on Thermal Quench in JET Disruptions

H. Strauss[1]
and JET Contributors[2]
[1] HRS Fusion, West Orange NJ, USA 07052
[2] See Joffrin et al 2019 (https://doi.org/10.1088/1741-4326/ab2276) for the JET team.

Abstract

Experimental data, simulations and theory are presented of a JET tokamak thermal quench. The emphasis is on the timescale of the bulk plasma thermal energy loss. The simulations suggest that the thermal energy loss is caused by a resistive wall tearing mode, and experimental data is consistent with this conclusion. The time scale of the thermal quench is the inverse of the mode growth rate.

1 Introduction

The thermal quench (TQ) phase of disruptions is not definitively understood. The TQ timescale is important because it determines the thermal load resulting from a disruption.

Experimental data, simulations and theory are presented of a JET tokamak locked mode thermal quench. The emphasis of this paper is on the timescale in which the bulk plasma thermal energy is lost. It has been widely accepted that a TQ is caused by growth of tearing [1] or neoclassical [2] tearing modes causing overlapping magnetic islands [3], producing stochastic magnetic field lines and rapid thermal transport [4]. It has also been suggested that a TQ is caused by a large amplitude magnetic island [5]. For these to be the main cause of energy loss, the wall must be highly conductive. Otherwise the plasma energy loss can be caused by a resistive wall tearing mode (RWTM) [6, 7, 8], a resistive plasma version of a resistive wall mode (RWM) [9, 10, 11].

The simulations indicate that the RWTM gives the best agreement with experimental data. The RWTM and RWM connect to tearing or kink modes respectively, which are marginally stable when the wall is perfectly conducting. The RWTM is more likely in this case than the RWM, since the plasma does not seem to be near ideal marginal stability.

Simulations were performed using the M3D [12] 3D resistive MHD code. The simulation model [13, 14] consists of resistive MHD with a resistive wall, including parallel and perpendicular thermal conduction. Radiation resulting from impurities will not be considered here. The mitigating effects of radiation have been investigated

in other simulations [15, 16, 17]. The simulations reported here are intended to identify the mode which causes the TQ.

Section 2 presents thermal quench data from JET pulse 81540. The TQ is correlated with the growth of locked mode magnetic field perturbations, on the resistive wall penetration timescale τ_{wall}. The growth time of the locked mode and the TQ time agree. Data from other disruption shots is consistent with these timescales. Section 3 describes nonlinear 3D MHD simulations. The disruption is initiated with fast MHD activity, with a timescale that is independent of the resistive wall time. This is followed by a quench of the total thermal energy. It is also shown that the fast initial stage of the disruption is not required for a RWTM to cause a TQ. Section 4 presents linear simulations which verify the RWTM dispersion relation. Also given is a derivation of the RWTM dispersion relation. An expression for the growth rate is found, which has not been given previously. In Section 5 a simple theory of the thermal quench is derived which is consistent with the simulations of Section 3. Section 6 compares the theory to JET data. The amplitude of the magnetic perturbations at the resistive wall agrees with the simulations and theory. Conclusions are presented in Section 7.

2 JET Experimental Data

About 16% of JET pulses with ITER like wall (ILW) had disruptions [19].

Fig.1 shows data from JET shot 81540. Shown is a fast ECE measurement [20] of T_e at $r \approx 0.2a, 0.45a, 0.6a$ where a is the minor radius. The ECE measurement has reasonably good time resolution, while the diamagnetic total energy measurement resolution is too slow to resolve the TQ. There is a faster time resolution signal, available for some shots. Also shown is the locked mode magnetic amplitude B_{ML} measured at saddle loops outside the vacuum vessel [20, 21, 22]. Fig.1(a) shows the ECE, plasma current $I_p(MA)$, and $B_{ML}(mT)$ signals from $t = 64.2s$ to $t = 64.35s$, surrounding the time of the thermal quench at about $t = t_{dis} = 64.297s$. There are fluctuations of the T_e signals, as well as in B_{ML}. The current spike is clearly seen.

Fig.1(b) shows some of the same data, expanded in time around $t = 64.2835s$, with time in units of the resistive wall penetration time $\tau_{wall} = 0.005s$[23, 24]. Also shown are fits to the data. Fit 1 is an exponential fit to the magnetic signal with constant growth rate $\propto \exp(\gamma t)$. From the fit it can be inferred that $\gamma \approx 2.73\tau_{wall}^{-1} \approx 475s^{-1}$. Fit 2 is to $T_e(0.2a)$ of the form $T_e(KeV) \propto 0.5\sigma(t)+.2$, where $\sigma(t) = \{1+\exp[(t-t_0)/\delta t)]\}^{-1}$, with $\delta t = 0.15\tau_{wall}$ and $t_0 = 2.59\tau_{wall}$. This implies a TQ time of about $\tau_{TQ} \approx 0.3\tau_{wall}$. The results of the two fits imply that

$$\tau_{TQ} \sim \gamma^{-1}. \tag{1}$$

This will be confirmed in the following. Fit 3 replaces the constant growth rate γ in fit 1 with a temperature dependent RWTM growth rate of the form $(T/T_0)^{-1/2}\gamma$, using fit 2 for the temperature. This gives a better fit at the beginning of the mode growth. The peak growth rate is about the same as for fit 1. If the mode is a RWTM, its growth rate scales as

$$\gamma\tau_A \propto S^{-1/3}S_{wall}^{-4/9} \tag{2}$$

otherwise it is a RWM mode with growth rate

$$\gamma\tau_A \propto S_{wall}^{-1}. \tag{3}$$

where $S = \tau_R/\tau_A$ is the Lundquist number, τ_R is the resistive diffusion time, $S_{wall} = \tau_{wall}/\tau_A = 7\times10^3$, τ_{wall} is the resistive wall magnetic penetration time, and $\tau_A = R/v_A$ is the Alfvén time, with major radius R and Alfvén speed v_A.

The locked mode signal is shifted by a time of order the skin time with respect to signals measured on the plasma side of the resistive wall. This is short compared to the mode growth time and will be neglected.

It is worthwhile to know if shot 81540 is representative. It is not feasible to fit all the data, so it must be analyzed numerically. The TQ time can be calculated from the disruption time $t = t_{dis}$, shown in Fig.1(b), which is included in the data. The time derivative of temperature is $\dot{T}$. The time at which the $\dot{T}$ reaches half its minimum value is $\dot{t}_{1/2}$. The TQ time is taken to be $(3/4)(t_{dis} - \dot{t}_{1/2})$, which approximately agrees with the fit above to shot 81540. To find the mode growth rate, the maximum value of B_{ML} is found at time $t = t_B$. The maximum time derivative $\dot{B}_{ML}$ is at time $t = \dot{t}_B$. The growth rate is taken as $\gamma = 2/(t_B - \dot{t}_B)$, in approximate agreement with the fit to shot 81540. This analysis is applied to the JET ILW disruption 2011-2016 database [19].

Shots are chosen that are labelled as unintentional disruptions. Not included are asymmetric vertical displacement events (AVDEs) and thermal quenches enhanced with massive gas injection (MGI) or pellet injection. Also excluded are shots in which the T_e data was not verified to be correct. The temperature is measured in several channels with a fast ECE signal. The data labelled 01, 20, 40, 50, 60, 70, 80, and 90 was averaged together. The channels correspond to data from different minor radius, which can vary from shot to shot. The averaging lets the signal be dominated by emission from smaller major radius which has less fluctuation than the temperature near the edge. Fig.2 gives the number of shots with values of τ_{TQ} and γ^{-1} in bins of width $0.1\tau_{wall}$. Typical values are about $\tau_{TQ} \approx \gamma^{-1} \approx 0.25\tau_{wall}$. This indicates that shot 81540 is reasonably representative of the database. The quantity $\delta t_{TQ-1/\gamma} = (\tau_{TQ} - 1/\gamma)/\tau_{wall}$ is the difference between the TQ time and the mode growth time for individual shots, which is small.

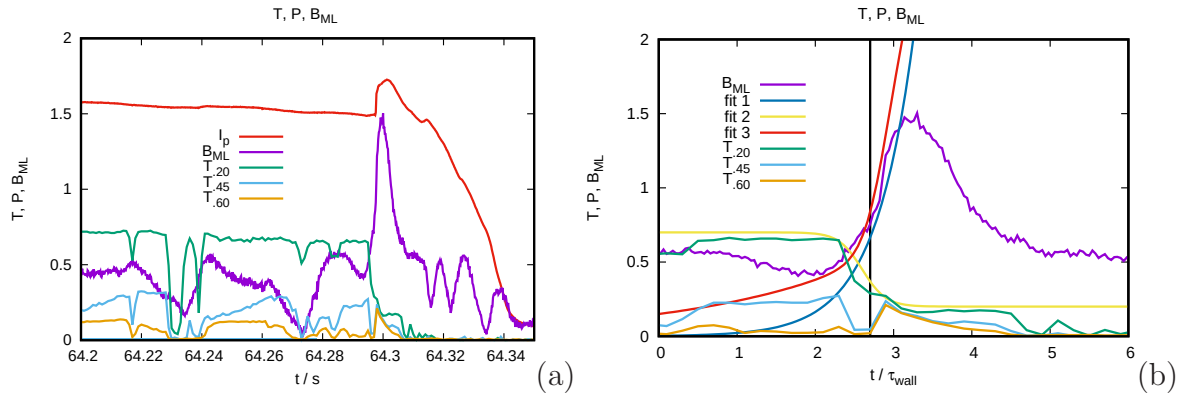

Figure 1: *JET shot 81540, showing time histories of (a) plasma current* $I_p(MA)$, $B_{ML}(mT)$, *fast ECE measurement of* $T_e(KeV)$ *at* $r = 0.2a, 0.45a, 0.6a$, *with time in sec. (b)* B_{ML} *and ECE measurements as in Fig.1 (a), with time in units of* $\tau_{wall} = 0.005s$, *centered at* $t = 64.2835s$. *The vertical line is the disruption time* t_{dis}.

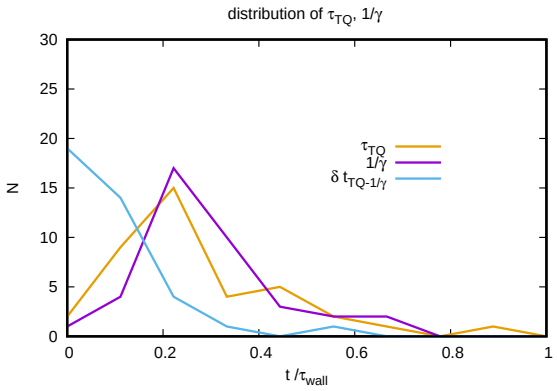

Figure 2: *(a) The distribution of* τ_{TQ} *and* γ^{-1} *as a function of* t/τ_{wall}. *The values of shot 81540 are typical values in the database. Only shots in which the* T_e *data was verified are included. The quantity* $\delta t_{TQ-1/\gamma} = (\tau_{TQ} - 1/\gamma)/\tau_{wall}$ *is the difference between the TQ time and the mode growth time for individual shots, and is relatively small.*

The magnetic data will be analyzed further in Section 6.

3 JET Thermal Quench Simulations

Simulations with M3D [12] were performed in order to find the dependence of γ and τ_{TQ} on τ_{wall}, which can distinguish RWTMs from RWMs. Tearing and neoclassical tearing modes do not depend on τ_{wall}. The simulations have initial Lundquist number $S = 10^6$ on axis, and resistive wall Lundquist number in a range of values around $S_{wall} = 7 \times 10^3$, the JET experimental value. The parallel thermal conductivity is $\chi_\parallel = 10R^2/\tau_A$, and the perpendicular thermal conductivity is $\chi_\perp = 10^{-4}a^2/\tau_A$. with a being the minor radius in the major radius direction. These choices will be justified below. The choice of $\chi_\perp$ is unrealistically large, but it is constrained by the need to maintain numerical stability. It is overwhelmed by parallel thermal conduction. The choice of $\chi_\parallel$ corresponds to an electron temperature T_e of about $100eV$ in the outer part of the JET plasma. When T_e is less than these temperatures, the edge thermal transport is dominated by resistive wall tearing modes (RWTMs).

It is noteworthy that edge cooling has been shown to destabilize tearing modes that cause mode locking in the termination phase of JET disruptions [25]. The edge cooling might serve as a precursor to the RWTMs described here.

The dependence on S_{wall} of the TQ is evidently caused by an increase of the normal magnetic field b_n at the wall. Here b_n is defined as the surface average along the wall of the root mean square value of the normal component of the perturbed, asymmetric magnetic field δB divided by the total field B, $b_n = (2\pi L)^{-1/2}[\oint d\phi \oint dl(\delta B_n/B)^2]^{1/2}$ where $L = \oint dl$.

In the simulations, the first wall boundary is treated as the resistive wall. The vacuum vessel is not taken into account. Theoretical analysis in Section 4 indicates (14),(15) that including the vacuum vessel might affect the growth rate, but would not fundamentally change the results. More realistic simulations are planned in which the vacuum vessel resistivity is taken into account.

Nonlinear simulations were initialized with an equilibrium reconstruction of JET shot 81540, at time $64.2s$. A different equilibrium reconstruction of the same shot is compared below and in Section 4.

The time evolution in the simulations involves two MHD events. In the equilibrium reconstruction, $q \approx 0.8$ initially. This causes a large $(1,1)$ mode, which causes a pressure pulse to spread to larger radii. This is a relatively fast process, independent of τ_{wall}. The associated magnetic perturbations cause a relatively slow loss of the total magnetic pressure. This is followed by the growth of a resistive wall tearing mode,

which is the main cause of the TQ. Without the RWTM, the TQ would be much slower. Fig.3(a) shows time history of the volume integral of pressure $P = \int pRdRdZd\phi$ in arbitrary units, and the normalized value of the root mean squared magnetic field at the wall b_n, for three cases with the same S and different S_{wall}. The case labelled P_3, b_3 has $S_{wall} = 10^3$, and similarly subscripts $4, 5$ correspond to $S_{wall} = 10^4, 10^5$. It can be seen that P_3 decays much more quickly than P_4, and P_4 decays much more quickly than P_5. Similarly, b_3 grows much more quickly than b_4, which in turn grows much more quickly than b_5. It is noticeable that there is a change in the rate of P decay, correlated with an increase in the growth of the amplitude of b_n. In addition there are exponential fits to $b_n = a_i \exp(\gamma_i t)$, labelled f_i, i =3, 4, 5 corresponding to b_i. The coefficients were chosen to align with the simulation data where the growth rate is largest. The fits indicate that $\gamma\tau_A \approx 0.054 S_{wall}^{-4/9}$.

The resistivity in the simulations varies as $T^{-3/2}$, and depends on the temperature T profile. Although the peak value of $S = 10^6$, at the $q = 2$ rational surface $r_s = 0.6a$, the value of $S = S_2 = 7 \times 10^4$. Using this value,

$$\gamma\tau_A = 2.2 S^{-1/3} S_{wall}^{-4/9} \tag{4}$$

assuming the $S^{-1/3}$ scaling from the linear simulations Fig.6(b) and theory (14).

Fig.3(b) collects the τ_{TQ} data for simulations with $S_{wall} = 10^3, 10^4, 10^5, 10^6$. The TQ time is measured as the time difference $(t_{30} - t_{90})/.6$, where t_{90} is the time at which the temperature is 90% of its peak value, and t_{30} is the time when it has 30% of its maximum value. It can be seen that there are two asymptotic dependencies of τ_{TQ} on S_{wall}. For smaller values of S_{wall}, the simulations are fit by a curve $\tau_{TQ}/\tau_A \approx 40 S_{wall}^{4/9}$. For larger S_{wall}, the simulations tend to $\tau_{TQ}/\tau_A = 8000 = const.$ The vertical line at $S_{wall} = 7 \times 10^3$ is the JET value. The asymptotic dependencies will be derived below (24). Fig.3(b) is consistent with $\tau_{TQ} = 0.4 S^{1/3} S_{wall}^{4/9} \tau_A$, or (1).

Fig.4 shows contour plots of temperature T in the $(R, Z, 0)$ plane from nonlinear simulations with $S_{wall} = 10^4$, labelled P_4 in Fig.3(a), at four times. The equilibrium T is shown in Fig.4(a). Fig.4 (b) shows T at $1943\tau_A$, just before the slope of P_4 sharply decreases. At this time P_4 is 70% of its initial value. Perturbations with $(m, n) = (2, 1)$ and $(3, 2)$ are visible. At(c) $t = 2403\tau_A$ during the middle of the TQ, P_4 has 30% of its initial value, and at (d) $t = 2879\tau_A$, it is near the end of the TQ.

The above simulations used an equilibrium reconstruction with $q < 1$ on axis initially. This caused a large $(1, 1)$ mode which produced a turbulent state. Another equilibrium reconstruction was used, in which $q = 1.05$ at the magnetic axis. This prevented the growth of the $(1, 1)$ mode which initiated the nonlinear disruption simulations. Fig.5(a) shows temperature contours at $t = 3381\tau_A$, initialized with the $q > 1$ equilibrium. There is no $(1, 1)$ and no initial turbulent state, but nonlinearly the in-

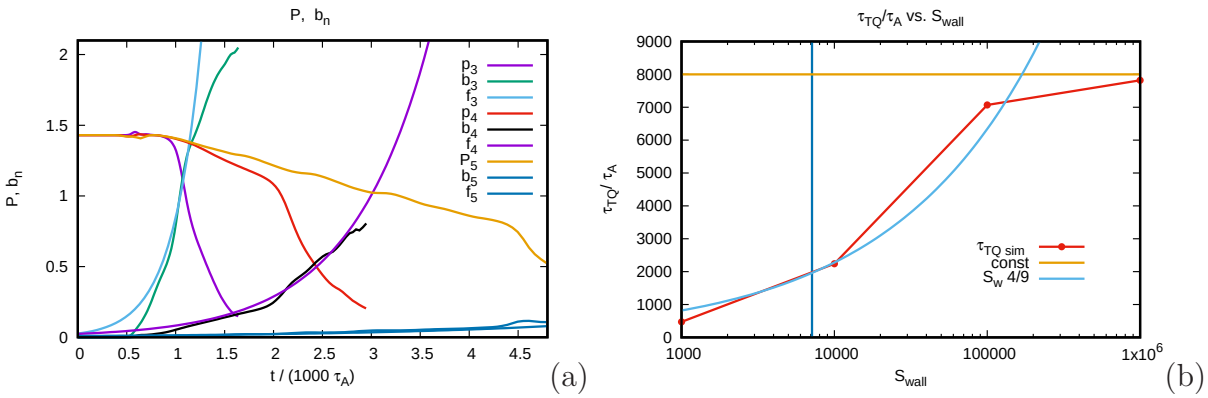

Figure 3: *(a) History of total pressure P and wall normal magnetic field perturbation b_n as a function of time. As b_n increases in time, P falls more rapidly. Three cases are shown, with $S = 10^6$, and $S_{wall} = 10^3, 10^4, 10^5$. The subscript in the label refers to S_{wall} such that P_a, b_a, f_a correspond to $S_{wall} = 10^a$, where f_a is an exponential fit to b_n. (b) τ_{TQ}/τ_A vs. S_{wall}. The fits are to $S_{wall}^{4/9}$ and constant.*

stability is similar to Fig.4. Fig.5(b) shows nonlinear simulations initialized with both equilibrium reconstructions. In both cases $S_{wall} = 7000$, the JET value. The total pressure P_1 and wall magnetic perturbation b_1 use the equilibrium with $q < 1$. The TQ has a slow timescale, produced by the internal MHD modes, and a faster timescale caused by the RWTM. This behavior is similar to the cases in Fig.3(a). The total pressure P_2 and wall magnetic perturbation b_2 use the equilibrium with $q > 1$. There are no modes except for the RWTM. The pressure P_2 is constant until the mode starts to grow. The absence of the internal modes causes a time delay in the TQ. The growth of b_1 and b_2 are similar, but with the time delay, because the RWTM grows from a smaller initial perturbation. Without the RWTM, there would be no TQ. This shows that the TQ is more like the single mode theory [5] than the overlapping island mode [3]. Even though in the $q < 1$ case this model may apply, the TQ of the bulk plasma energy is caused by a large RWTM.

4 Linear stability

Linear stability calculations indicate the presence of the resistive wall tearing mode. To carry out the linear simulations, the $q > 1$ equilibrium reconstruction was used, in which $q = 1.05$ at the magnetic axis, to eliminate the $(1, 1)$ mode. Fig.6 (a) shows the linear growth rate as a function of S_{wall} which is consistent with $\gamma\tau_A \propto S_{wall}^{-4/9}$, where $S = 10^6$. A least squares fit [26] gives $\gamma\tau_A \propto S_{wall}^{-0.37}$. Fig.6 (b) shows linear growth

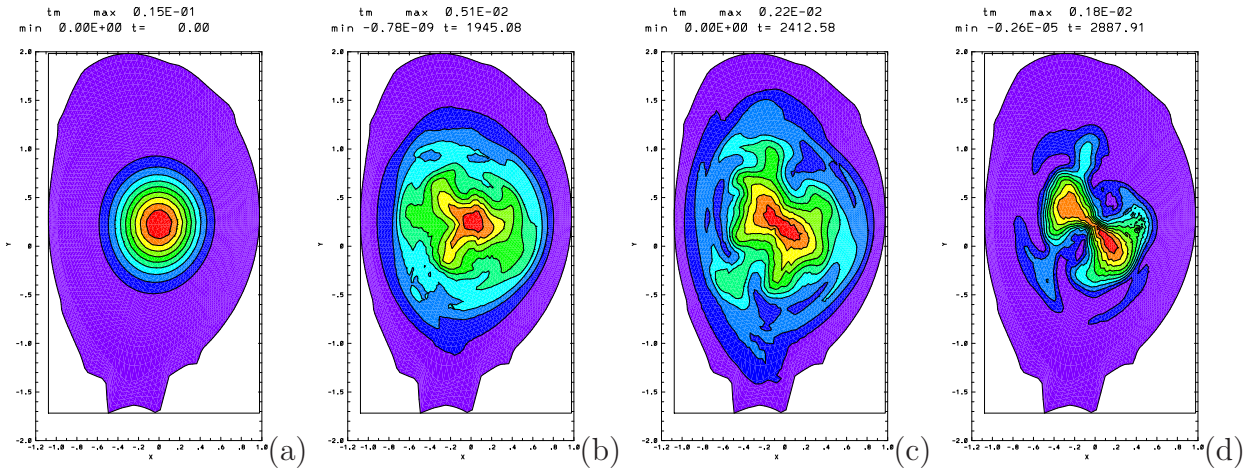

Figure 4: *Simulation of JET shot 81540, with* $S_{wall} = 10^4$. *The time history is shown in Fig.3(a). (a) initial temperature* T. *(b) temperature* T *at* $t = 1945\tau_A$, *showing* $(2,1)$ *and* $(3,2)$ *magnetic perturbations. At this time* $P \approx 70\%$ *of its initial value. (c)* T *at* $t = 2428\tau_A$. *At this time* $P \approx 30\%$ *of its initial value. (d)* T *at* $t = 2888\tau_A$, *at the end of the simulation.*

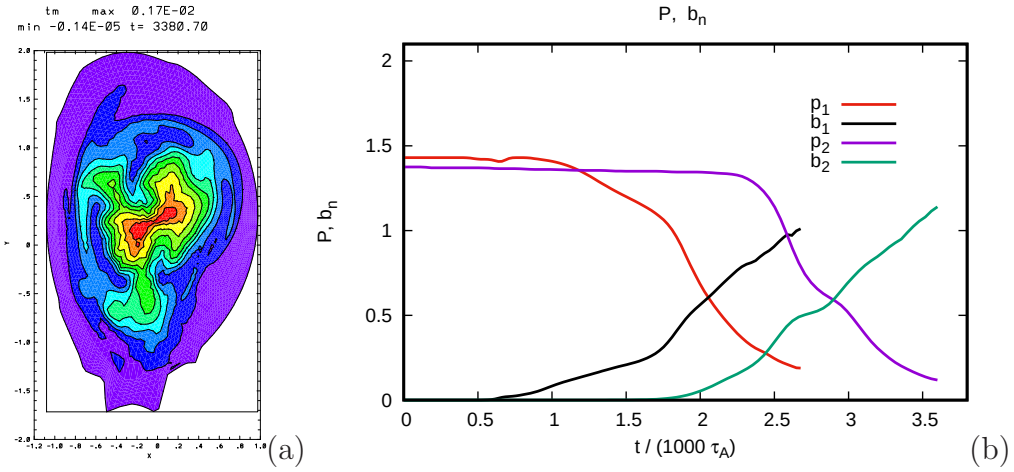

Figure 5: *(a) Plot of temperature at* $t = 3381\tau_A$ *in a simulation with* $q > 1$ *initially. The plot is qualitatively similar to Fig.4(c). (b) nonlinear simulations comparing the equilibria with initial on axis* $q > 1$ *and* $q < 1$ *as in Fig.3(a). In these simulations* $S_{wall} = 7000$, *the experimental value. When* $q > 1$, *there is no other instability besides the RWTM, and the TQ is produced only by the RWTM.*

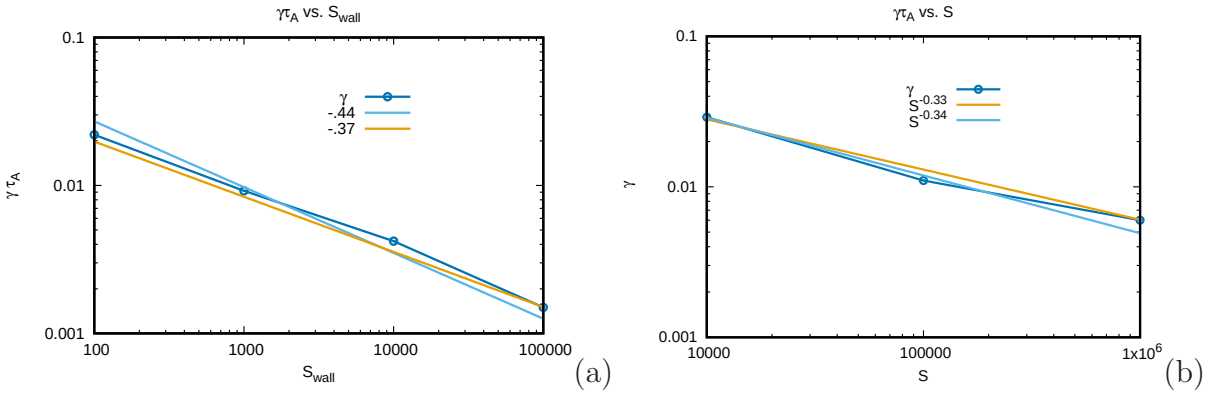

Figure 6: *(a) Linear growth rate γ as a function of S_{wall}, from simulations of JET shot 81540 . The growth rate is consistent with $S_{wall}^{-4/9}$. (b) Growth rate as a function of S, consistent with $S^{-1/3}$ scaling.*

rate as a function of S, which is consistent with $\hat{\gamma} \propto S^{-1/3}$, where $S_{wall} = 10^3$. The same fit gives $\gamma\tau_A \propto S^{-0.34}$. Combining the fits to these curves is consistent with the RWTM scaling (2).

The growth rate can be obtained from a limit of the dispersion relation obtained in [6]. Here another derivation is given. The linear growth rate of the tearing mode [27] is given by

$$\gamma\tau_A = 0.55 \left(\frac{mq'r_s}{q^2}\right)^{2/5} (\Delta' r_s)^{4/5} S^{-3/5} \tag{5}$$

where r_s is the rational surface and m is the poloidal mode number. For simplicity, a zero pressure circular large aspect ratio geometry is assumed, with no toroidal current for $r > r_s$. The task is to obtain Δ' when there is a resistive wall at $r = r_w$. For $r_s < r < r_w$, $\psi = Ar^m + Br^{-m}$. At $r = r_s$, $\Delta' = \Delta'_+ - \Delta'_-$. The contribution Δ'_- from the interior $r < r_s$ is assumed known. The exterior part is given by

$$\Delta'_+ = \frac{\psi'_+}{\psi_+} = \frac{m}{r_s} \frac{Ar_s^m - Br_s^{-m}}{Ar_s^m + Br_s^{-m}}. \tag{6}$$

For $r_w < r$, $\psi = Fr^{-m}$. At the wall, continuity of ψ requires

$$Fr_w^{-m} = Ar_w^m + Br_w^{-m} \tag{7}$$

and the evolution of ψ due to the resistive wall is given by [18]

$$\gamma\psi_w = \frac{\eta_{wall}}{\delta_{wall}}(\psi'_{w+} - \psi'_{w-}) = \frac{m}{\tau_{wall}}(-Fr_w^{-m} - Ar_w^m + Br_w^{-m}) \tag{8}$$

Eliminating F between (7) and (8) to obtain A/B and substituting in (6),

$$\frac{r_s}{m}\Delta'_+ = \frac{r_s^{2m} + r_w^{2m}(1+\delta)}{r_s^{2m} - r_w^{2m}(1+\delta)} \tag{9}$$

where

$$\delta = \frac{2m}{\gamma \tau_{wall}} \tag{10}$$

Let $\gamma\tau_{wall} \gg 1$, so that $1 \gg \delta$, and expand (9) in δ,

$$\frac{r_s}{m}\Delta'_+ = -\frac{r_w^{2m} + r_s^{2m}}{r_w^{2m} - r_s^{2m}} \left(1 - 2\delta \frac{r_s^{2m} r_w^{2m}}{r_w^{4m} - r_s^{4m}}\right) \tag{11}$$

Now let it be assumed that Δ' is small. The first term in (11), which is negative, is assumed to nearly cancel Δ'_-, so that $\Delta' = 0$ if the wall is an ideal conductor, $\delta = 0$. The RWTM is marginally stable for an ideal wall. Then

$$r_s \Delta' = \frac{4m^2 f}{\gamma \tau_{wall}}. \tag{12}$$

where

$$f = \frac{(r_s/r_w)^{2m}}{[1 - (r_s/r_w)^{2m}]^2} \tag{13}$$

Substituting in the tearing dispersion relation (5) gives, with $m = q = 2$,

$$\gamma \tau_A = c_0 S^{-1/3} S_{wall}^{-4/9} \tag{14}$$

where

$$c_0 = 2.46 \left(\frac{q' r_s}{q}\right)^{2/9} f^{4/9} \tag{15}$$

This gives the scaling of γ with S, S_{wall}, and r_s/r_w. For example, let $r_s = .6a$, $r_w = a$, then $f^{4/9} = 0.45$; if $r_s = .8a$, $r_w = 1.4a$, the same f is obtained. For $(r_s/r_w)^4 \ll 1$, $f^{4/9} \approx (r_s/r_w)^{16/9}$.

The nonlinear simulations show that the linear dispersion relation holds even as the mode grows to large amplitude. This is analogous to the resistive $(1,1)$ internal kink [28], which grows at the linear rate to large amplitude, and also has a $S^{-1/3}$ scaling of the growth rate.

It is worth comparing the growth rate of the RWTM to the resistive wall mode (RWM) [9, 10, 11]. The RWM growth rate is $\gamma_{RWM} = c_2 S_{wall}^{-1}$. This is less than the RWTM growth rate if $c_0 S_{wall}^{-4/9} S_{-1/3} > c_2 S_{wall}^{-1}$. or

$$S_{wall} > \left(\frac{c_2}{c_0}\right)^{9/5} S^{3/5} \tag{16}$$

This is essentially the validity condition for (12). If $S = 10^6$, then (16) requires $S_{wall} > 4000(c_2/c_0)^{9/5}$. If $c_2 < c_0$ this criterion is easily satisfied. For sufficiently large S_{wall}, the RWTM has a larger growth rate that the RWM. It should be noted that the RWTM and RWM occur in different instability regimes. The RWTM connects to a marginally stable tearing mode, while the RWM connects to a marginally stable ideal kink mode.

5 Thermal Quench Theory

The simulation results can be analyzed as follows. The analysis shows how the two limiting dependencies of τ_{TQ} seen in Fig.3(b) can be obtained from a model of parallel thermal conduction. During the TQ, heat travels along the magnetic field as

$$\frac{\partial T}{\partial t} = \frac{1}{r}\frac{\partial}{\partial r} r(\chi_{\parallel} b_r^2 + \chi_{\perp}) \frac{\partial T}{\partial r} \tag{17}$$

where b_r is the normalized asymmetric radial magnetic field, assuming circular flux surfaces for simplicity. The field is assumed stochastic, so there is an average radial magnetic field. Integrating, the total temperature is given by

$$\frac{\partial < T >}{\partial t} = a(\chi_{\parallel} b_n^2 + \chi_{\perp}) T' \tag{18}$$

where $< T >= \int T r dr$, $T' = \partial T/\partial r$ at $r = a$, and $b_n = b_r$ at the wall. Assume that $T'/ < T >= -a^{-3}$. The normal magnetic field at the wall is

$$b_n = b_{n0} \exp(\gamma t) \tag{19}$$

where b_{n0} is the initial amplitude, and γ is the RWTM growth rate.

Neglecting $\chi_{\perp}$, substituting for b_n in (18) and integrating in time, from $t = 0$ to τ_{TQ},

$$1 = \frac{\chi_{\parallel} b_n^2}{2\gamma a^2} [\exp(2\gamma \tau_{TQ}) - 1] \tag{20}$$

This gives

$$t_{TQ} = \frac{1}{2\gamma} \ln\left(1 + \frac{2}{\alpha}\right) \tag{21}$$

which has two limits,

$$t_{TQ} = \begin{cases} (2\gamma)^{-1} \ln[2/\alpha] & \gamma t_{TQ} \sim 1 \\ a^2/(\chi_{\parallel} b_n^2) & \gamma t_{TQ} << 1. \end{cases} \tag{22}$$

where

$$\alpha = \frac{\chi_{\parallel} b_{n0}^2}{a^2 \gamma} \tag{23}$$

An *ad hoc* fit to the simulations is

$$\tau_{TQ} \approx \left(\frac{1}{\gamma}, \frac{a^2}{\chi_{\parallel} b_{n0}^2}\right)_{min} \tag{24}$$

consistent with (1).The limits correspond to the case when the RWTM is dominant, and when its growth rate is small.

6 Comparison with experiment

The magnetic perturbations are measured by saddle loops [21, 22] placed at a maximum major radius of $R_{loop} = 4.4m$, the magnetic axis is approximately at $R_0 = 2.9m$, and the major radius of the wall is $R_{wall} = R_0 + 1m$. The effective cylindrical radius of the wall is $r_{wall} = R_{wall} - R_0 = 1m$, and of the saddle loops is $r_{loop} = R_{loop} - R_0 = 1.4m$. Between the wall and the loops, the flux varies as r^{-2} and the normal magnetic field as r^{-3}. The normal field at the wall is $(r_{loop}/r_{wall})^3 = 2.7$. At the wall, $b_n = 2.7B_{ML}/B_0 = 1.1B_{ML}/(T)$, with $B_0 = 2.4T$. Taking the difference of peak and initial values of $B_{ML} = (1.4 - 0.4)mT$ in Fig.1 then $b_n = 1.1 \times 10^{-3}$. In Fig.5 the peak value of $b_n = 1.2 \times 10^{-3}$, consistent with the data.

To assess whether the theoretical parameters are consistent with experiment, let $T_e = T_0(100eV)$, $n = n_0(10^{14}cm^{-3})$, $a = a_0(m)$, $B = 10^4 B_0(T)$, $R/a = 3$, $b_n = 10^{-3}b_0$ $\mu = m_i/m_p$, $\lambda = 15$, and $S_{wall} = 10^4 S_{w0}$. Then [29]

$$\chi_{\parallel} = 2.1 v_{te}^2 \tau_e = 0.9 \times 10^{11} \frac{T_0^{5/2}}{n_0} cm^2/s \tag{25}$$

taking $\chi_{\parallel} = (2/3)\kappa_{e\parallel}/n_e$. The Alfvén time is

$$\tau_A = \frac{R}{v_A} = 1.4 \times 10^{-6} \frac{a_0(\mu n_0)^{1/2}}{B_0} s \tag{26}$$

In JET shot 81540 , with $B_0 = 2.4, a_0 = 1, \mu = 2, n_0 = 0.65$ then $\tau_A \approx 0.7 \times 10^{-6} s$. Normalizing $\chi_{\parallel}$ to a^2/τ_A and multiplying by b_n^2,

$$\frac{\chi_{\parallel} \tau_A b_n^2}{a^2} = 1.3 \times 10^{-5} \frac{b_0^2 T_0^{5/2}}{a_0 B_0} \left(\frac{\mu}{n_0} \right)^{1/2}. \tag{27}$$

The perpendicular diffusion coefficient can be taken as the Bohm value,

$$\chi_{\perp} = \frac{1}{4} \rho_e v_{te} = 1.2 \times 10^4 cm^2/s \approx 1m^2/s,$$

a typical value of turbulent diffusion coefficient. This is much smaller than the parallel diffusion and will be neglected. Next the resistive diffusion time is $\tau_R = a^2/\eta = a^2 \omega_{pe}^2 \tau_e / c^2$ giving

$$S = \frac{\tau_R}{\tau_A} = 6 \times 10^5 \frac{a_0 B_0 T_0^{3/2}}{\sqrt{\mu n_0}} \tag{28}$$

The value of $\gamma \tau_A$ of a RWTM is

$$\gamma \tau_A = c_0 S_{wall}^{-4/9} S^{-1/3} = 2 \times 10^{-4} \frac{c_0 (\mu n_0)^{1/6}}{(a_0 B_0)^{1/3} S_{w0}^{4/9} T_0^{1/2}}. \tag{29}$$

Let α be the ratio of the two terms in (23),

$$\alpha = 6.5 \times 10^{-2} \frac{b_0^2 T_0^3 \mu^{1/3} S_{w0}^{4/9}}{c_0 (n_0 a_0 B_0)^{2/3}} \tag{30}$$

For JET parameters $S_{w0} = 0.7$, $\mu = a_0 = n_0 = 1$, $B_0 = 2$,

$$\alpha = 0.28 \frac{b_0^2}{c_0} = 0.3, \tag{31}$$

taking $T_0 = c_0 = b_0 = 1$. This gives $\ln(2/\alpha) \approx 2$ in (22), in agreement with (24).

The ratio α decreases rapidly as T^{-3}.

7 Discussion and Conclusion

To summarize, experimental data, simulations, and theory of the TQ were presented. The results were were obtained for a particular JET pulse 81540, which is a locked mode pulse, like most ILW JET disruptions [22]. The data shows that the thermal quench occurs in a fraction of the resistive wall time. In shot 81540, $\tau_{TQ} \approx 0.3\tau_{wall}$. The growth rate γ of the mode that terminates the TQ is $\gamma \approx \tau_{TQ}^{-1}$. The growth rate of the mode appears to scale as $\gamma \propto T_e^{-1/2}$. Analysis of shots in the JET ILW 2011-16 disruption database show that the TQ time and mode growth rate have typical values similar to shot 81540.

These features of the data were also found in simulations. The growth rate of the mode that caused the TQ had $\gamma\tau_A \approx 2S^{-1/3}S_{wall}^{-4/9}$, which is the growth rate of a RWTM. The TQ time satisfied $\gamma\tau_{TQ} \approx 1$.

It was verified that the amplitude of the modes is consistent with the experimental data, such that the locked mode amplitude at the saddle coils is of order $1mT$.

Simulations were done with two equilibrium reconstructions. In one, initially $q < 1$, leading to a large internal kink and an outward pressure pulse, which produced magnetic perturbations. This was followed by growth of the RWTM, which caused the quench of the bulk plasma energy. In the other reconstruction, $q > 1$ initially and the plasma was unstable only to the RWTM. Nonlinear simulations verified that the RWTM by itself was enough to cause a TQ. Linear simulations verified the S and S_{wall} dependence of the RWTM.

A linear analysis of the RWTM was carried out which verified the scaling with $\gamma \propto S^{-1/3}S_{wall}^{-4/9}$. This expression for the growth rate has not been given previously. It includes the dependence of the growth rate on the ratio of the rational surface radius to the resistive wall radius.

A simple theory obtained the asymptotic dependence of τ_{TQ} on the mode growth as well as parallel thermal conduction when the mode growth rate is small. The theory

was compared with experimental data, verifying that the theory and simulations were in agreement for the appropriate parameters.

The results are relevant to JET locked mode disruptions. It is not known how prevalent the RWTM is in other experiments, especially in ITER. It would be desirable to carry out simulations to find out.

The dependence of τ_{TQ} on S_{wall} is potentially mitigating for ITER, with a longer S_{wall} than in JET. The TQ time might be increased from $1.5ms$ in JET to $5ms - 10ms$ in ITER. This could relax the requirements for the ITER disruption mitigation system and runaway electron avoidance. On the other hand, higher temperatures in ITER might suppress the effect of the RWTM. It is hoped to investigate the matter in future work.

Acknowledgment The help of S. N. Gerasimov with obtaining and analyzing the JET data, and Hongjuan Sun for validating temperature data, is acknowledged. This research was supported by USDOE grant DE-SC0020127. This work has been carried out within the framework of the EUROfusion Consortium and has received funding from the Euratom research and training programme 2014-2018 and 2019-2020 under grant agreement No 633053. The views and opinions expressed herein do not necessarily reflect those of the European Commission.

Data availability statement The data that support the findings of this study are available from the corresponding author upon reasonable request and with the permission of JET authorities.

References

[1] P. H. Rutherford, Phys. Fluids **16**, 1903 (1973).

[2] Z. Chang, J. D. Callen, E. D. Fredrickson, R. V. Budny, C. C. Hegna, K. M. McGuire, M. C. Zarnstorff, and the TFTR Group, Phys. Rev. Lett. **74**, 4663 (1995).

[3] B. V. Waddell, B. Carreras, H. R. Hicks, J. A. Holmes, and D. K. Lee, Phys. Rev. Lett. **41**, 1386 1978.

[4] A. B. Rechester and M. N. Rosenbluth, Phys. Rev. Lett. 40, 38 1978

[5] R. B. White, D. A. Monticello, and M. N. Rosenbluth, Simulation of large magnetic islands: a possible mechanism for a major tokamak disruption, Phys. Rev. Lett. **39**, 1618 (1977)

[6] John A. Finn, Stabilization of ideal plasma resistive wall modes in cylindrical geometry: the effect of resistive layers, Phys. Plasmas 2, 3782 (1995)

[7] R. Betti, Beta limits for the n = 1 mode in rotating - toroidal - resistive plasmas surrounded by a resistive wall, Phys. Plasmas 5, 3615 (1998).

[8] T.C. Hender, C.G. Gimblett, D.C. Robinson, Effects of a resistive wall on magnetohydrodynamic instabilities, Nucl. Fusion **29** 1279 (1989).

[9] A. Bondeson and D. J. Ward, Stabilization of external modes in tokamaks by resistive walls and plasma rotation, Phys. Rev. Lett. 72, 2709 (1994).

[10] Richard Fitzpatrick, A simple model of the resistive wall mode in tokamaks, Phys. Plasmas **9** 3459 (2002).

[11] Fabio Villone, Yueqiang Liu, Guglielmo Rubinacci and Salvatore Ventre, Effects of thick blanket modules on the resistive wall modes stability in ITER, Nucl. Fusion 50 (2010) 125011.

[12] W. Park, E. Belova, G. Y. Fu, X. Tang, H. R. Strauss, L. E. Sugiyama, Plasma Simulation Studies using Multilevel Physics Models, Phys. Plasmas **6** 1796 (1999).

[13] H. Strauss, E. Joffrin, V. Riccardo, J. Breslau, R. Paccagnella, and JET Contributors, Comparison of JET AVDE disruption data with M3D simulations and implications for ITER, Phys. Plasmas **24** 102512 (2017).

[14] H. Strauss, E. Joffrin, V. Riccardo, J. Breslau, R. Paccagnella, G.Y. Fu, and JET contributors, Reduction of asymmetric wall force in JET and ITER disruptions including runaway electrons, Phys. Plasmas **27** 022508 (2020)

[15] V. A. Izzo, D. G. Whyte, R. S. Granetz, P. B. Parks, E. M. Hollmann, L. L. Lao, J. C. Wesley, Magnetohydrodynamic simulations of massive gas injection int Alcator C - Mod and DIII-D plasmas, Phys. Plasmas **15**, 056109 (2008).

[16] N.M. Ferraro, B.C. Lyons, C.C. Kim, Y.Q. Liu and S.C. Jardin, 3D two-temperature magnetohydrodynamic modeling of fast thermal quenches due to injected impurities in tokamaks, Nucl. Fusion **59** (2019) 016001.

[17] E. Nardon, A. Fil, M. Hoelzl, G. Huijsmans and JET contributors, Progress in understanding disruptions triggered by massive gas injection via 3D non-linear MHD modelling with JOREK, Plasma Phys. Control. Fusion **59** 014006 (2017).

[18] H. Strauss, MHD Simulations with Resistive Wall and Magnetic Separatrix, Computer Physics Communications 164, 40 (2004).

[19] S.N. Gerasimov, P. Abreu, G Artaserse, M. Baruzzo, P. Buratti, I.S. Carvalho, I.H. Coffey, E. de la Luna, T.C. Hender, R.B. Henriques, R. Felton, S. Jachmich, U. Kruezi, P.J. Lomas, P. McCullen, M. Maslov, E. Matveeva, S. Moradi, L. Piron, F.G. Rimini, W. Schippers, G. Szepesi, M. Tsalas, L.E. Zakharov and JET

Contributors, Overview of disruptions with JET-ILW, Nucl. Fusion **60** 066028 (2020).

[20] S.N. Gerasimov, P. Abreu, G. Artaserse, P. Buratti, I.S. Carvalho, E. de la Luna, A.R. Field, E. Giovannozzi, T.C. Hender, R.B. Henriques, P.J. Lomas, E. Matveeva, S. Moradi, L. Piron, F.G. Rimini, H. Sun, G. Szepesi, L.E. Zakharov and JET Contributors, Locked mode and disruptions in JET-ILW, 46th EPS Conf. Plasma Physics (Milan, Italy, 8–12 July 2019) P1.1056 (http://ocs.ciemat.es/EPS2019PAP/pdf/P1.1056.pdf)

[21] S. N. Gerasimov, P. Abreu, M. Baruzzo, V. Drozdov, A. Dvornova, J. Havlicek, T. C. Hender, O. Hronova, U. Kruezi, X. Li, T. Markovic, R. Panek, G. Rubinacci, M. Tsalas, S. Ventre, F. Villone and L. E. Zakharov, JET and COMPASS asymmetrical disruptions, Nucl. Fusion **55** 113006 (2015).

[22] P.C. de Vries, G. Pautasso, E. Nardon, P. Cahyna, S. Gerasimov, J. Havlicek, T.C. Hender, G.T.A. Huijsmans, M. Lehnen, M. Maraschek, T. Markovic, J.A. Snipes and the COMPASS Team, the ASDEX Upgrade Team and JET Contributors, Scaling of the MHD perturbation amplitude required to trigger a disruption and predictions for ITER, Nucl. Fusion **56** 026007 (2016).

[23] V. Riccardo, T. C. Hender, P. J. Lomas, B. Alper, T. Bolzonella, P. de Vries, G. P. Maddison and the JET EFDA Contributors, Analysis of JET halo currents, Plasma Phys. Control. Fusion **46**, 925 (2004).

[24] R. Albanese, M. Mattei and F. Villone, Prediction of the growth rates of VDEs in JET, Nucl. Fusion **44** 999 (2004)

[25] G. Pucella, P. Buratti, E. Giovannozzi, E. Alessi, F. Auriemma, D. Brunetti, D. R. Ferreira, M. Baruzzo, D. Frigione, L. Garzotti, E. Joffrin, E. Lerche, P. J. Lomas, S. Nowak, L. Piron, F. Rimini, C. Sozzi, D. Van Eester, and JET Contributors, Tearing modes in plasma termination on JET: the role of temperature hollowing and edge cooling, Nucl. Fusion (2021) https://doi.org/10.1088/1741-4326/abe3c7

[26] http://gnuplot.sourceforge.net/docs_4.2/node84.html

[27] H. P. Furth, J. Killeen, and M. N. Rosenbluth, Phys. Fl. **6**, 459 (1963).

[28] B. B. Kadomtsev, Fiz. Plazmy **1** 710 (1975) [Sov. J. Plasma Phys. **1** 389 (1976); B. Coppi, R. Galvao, R. Pellat, M. N. Rosenbluth, and P. H. Rutherford, Resistive internal kink modes, Fiz. Plasmy **2**, 961 (1976) [Sov. J. Plasma Physics **2**, 533 (1976)]; W. Park and D. A. Monticello, Nucl. Fusion **30**, 2413 (1990).

[29] J. D. Huba, NRL Plasma Formulary, Naval Research Laboratory (Washington DC) 2007